INVESTIGATION OF HIGH LYING STATES USING SINGLE NUCLEON TRANSFER REACTIONS

By

Gwang Ho Yoo

A DISSERTATION

Submitted to
Michigan State University
in partial fulfillment of the requirements
for the Degree of

DOCTOR OF PHILOSOPHY

Department of Physics and Astronomy

1992

ABSTRACT

INVESTIGATION OF HIGH LYING STATES USING SINGLE NUCLEON TRANSFER REACTIONS

By

Gwang Ho Yoo

The reactions (^{7}Li,^{6}Li), (^{7}Li,^{6}He), (^{7}Li,^{8}Li), (^{12}C,^{13}N) and (^{12}C,^{13}C) have been measured at 30 MeV/n on the targets ^{90}Zr, ^{91}Zr, ^{89}Y, ^{208}Pb, ^{209}Bi and ^{207}Pb in order to investigate high lying states. Particles were analyzed using the S320 magnetic spectrograph. In each reaction, the measured spectra were plotted both as a function of the reaction Q – value and as a function of the excitation energy. A preference for the excitation of high spin states with no spin flip was observed. Broad resonance like peaks were observed in both proton and neutron stripping reactions at excitation energies close to the excitation energy of the giant quadrupole resonance. Comparison of reaction Q – values and the excitation energy spectra suggests that these broad peaks are due to the excitation of single particle states rather than a collective giant resonance. The existence of an extra particle or hole outside closed shell nuclei does not change the strengths of these broad peaks significantly, but does change the excitation energies significantly in some cases. Shell model calculations carried out in the ^{208}Pb region support this conclusion. Substantial backgrounds were observed in these stripping reactions. Calculations of these underlying backgrounds were carried out with the Serber model and with a semi-classical theory developed

by Brink and Bonaccorso. The Serber model calculations do not match the shape of the experimental spectra except at the very high excitation energies (> 35 MeV) in proton stripping. The Brink-Bonaccorso model, does match the shape of the experimental spectra for neutron stripping reactions very well although it does not agree with the shape for the proton stripping case. The Brink-Bonaccorso model, also, predicts that for these bombarding energies, only 20% of the continuum arises from projectile breakup and 80% arises from the excitation of compound states in the residual nucleus. Strong peaks observed the (^{12}C,^{13}C) reaction on both ^{90}Zr and ^{208}Pb region targets appear to arise from the mutual excitation of bound $2s_{1/2}$, $1p_{3/2}$ and $1d_{5/2}$ excited states in ^{13}C along with low lying states of the residual nuclei. Broad peaks are observed for the (^{12}C,^{13}N) reaction on the ^{208}Pb, ^{209}Bi and ^{207}Pb targets at excitation energies about 18 MeV. The origins of these structures are not understood clearly.

ACKNOWLEDGEMENTS

I would like to thank my advisor Professor G. M. Crawley for his guidance and direction. His constant advice and support played the most important role to complete this thesis. Professors P. Danielewicz, B. Lynch, P. Schroeder and D. Stump are also thanked for their guidance and support.

There are many people whom I would like to thank: Prof. J. Finck for his reading and correcting my writting, Dr. J. S. Winfield for his help to prepare the experiment and for many discussions about the analysis, Profs. D. Brink and A. Bonaccorso for their help to calculate the background for the continuum states, Prof. A. Brown for his help to understand and use the Shell Model code and Prof. D. Cha for the fruitful discussions about the contents of my thesis, Dr. S. Gales, Dr. N. Orr and J. Yurkon for their help during the experiment. L. Zhao is thanked for the discussions on several questions. This work would have been impossible without the help of these people.

I would also like to thank all my friends, K. Joh, J. Kim, J. Yee and D. Jeon for their encouragement to finish my work at the NSCL.

I owe a large debt to my family, especially my parents, my wife's parents and my brothers who loved, encouraged and helped me to study throughout the years. Finally, I am specially grateful to my two children, Sung Hyun and Seok Hyun, and my wife, Soo Gyung for their endless understanding, patience and love.

Contents

List of Tables

List of Figures

Chapter 1

Introduction

1.1 Motivation

The study of deep lying hole states and high lying particle states has been an interesting area of research and many investigations have been carried out particularly for nuclei near closed shells. These studies provide information on the strength distribution (position and width) of high lying single particle states, deep lying single hole states, and the mechanism that spreads these states. Such information is useful for calculations of more complicated excitations, such as giant resonances (GR) and multiple particle/hole excitations. The single particle transfer reaction is a simple method for studying hole states in heavy target nuclei compared to knock out reactions such as $(e, e'p)$ and $(p, 2p)$ which require coincidence measurements, and is the only way of observing particle states at high excitation in heavy nuclei. This method has proved successful particularly at lower excitation energy for light ion induced reactions such as (p,d), (^{3}He,^{4}He) and (^{4}He,^{3}He) [Kasa 83, Gerl 75, Mass 86]. These experiments found single particle and single hole state strengths ranging from discrete peaks at low excitation to large broad peaks at high excitation energy. The couplings to more complicated collective excitations such as phonon excitations were found to play a very important role in spreading the strength of the simpler states [Gale 85].

Unfortunately, in light ion reactions the poor peak to background ratio makes it difficult to use these reactions to study highly excited states. The major source of the background at high excitation energy is the breakup of the projectile. This background must be subtracted to obtain the strength of the peaks of interest, and has usually been estimated empirically. Several theories have been proposed to calculate the background. For example, the Serber Model [Serb 48] explains the background very well in light ion induced nuclear reactions, but it does not explain the background well in heavy ion induced reactions. A semi-classical theory developed by Brink and Bonaccorso [Bona 85, Bona 88] explains the shape of the background very well in a number of neutron stripping reactions, although it does less well in proton stripping reactions. Both of these models will be discussed in more detail in chap. 6 [Wu 78, Wu 79, Bona 91].

Heavy ion reactions at high energies are expected to be more selective of high spin states which might therefore become stronger relative to the background [Brin 72] than in light ion induced reactions. However, to make use of these reactions for studying high lying states, some questions remain to be answered. Recently, it has been reported in the ^{208}Pb(^{20}Ne,^{19}Ne) and the ^{90}Zr(^{20}Ne,^{19}Ne) reactions at 25, 30, 40 MeV/n [Fort 90, Fras 87] and in the ^{208}Pb(^{12}C,^{11}C) reaction at 40 MeV/n [Merm 88], that large broad peaks were observed at excitation energies which are close to the excitation energies of the giant quadrupole resonance (GQR), viz. 10.5 MeV for ^{208}Pb and 13.5 MeV for ^{90}Zr. A broad peak was observed at a similar energy in the (^{4}He,^{3}He) reaction at 46 MeV/n on a ^{208}Pb target [Mass 86] and in the (^{16}O,^{15}O) reaction at 20 MeV/n on a ^{197}Au target [Olme 78]. However, the broad peaks in the vicinity of the GQR were not observed in the (^{7}Li,^{6}Li) and (^{16}O,^{15}O) reactions at 20 MeV/n on a ^{208}Pb target [Becc 87, Olme 78] nor in the (^{4}He,^{3}He) reaction at 46 MeV/n on a ^{120}Sn target [Gale 85]. When these broad peaks are observed in transfer reactions,

they have excitation energies, widths and strengths consistent with the known GR states [Fort 90, Fras 87, Fras 89, Duff 86, Olme 78, Gale 91]. (Some experimental transfer reaction spectra with broad peaks are shown in fig. 1.1.) Whether these peaks are from the excitation of GR states or from broad single particle states is not clear.

The GR is known to be a $1p-1h$ excitation in which many nucleons are involved. Most information on GRs has been obtained through the inelastic scattering of light ions [Youn 76], and heavy ions [Fras87a, Suom 89, Suom 90]. So far the evidence for the excitation of GR states by transfer reactions is less convincing. According to RPA theory, however, closed shell nuclei may contain some admixtures of $p-h$ states in the ground state [Ring 80]. When a nucleon is transferred to these closed shell target nuclei, this nucleon may couple to the existing hole state in the target by a single step mechanism and thus excite a component of a GR. A similar processes of forming a GR may be possible by a pickup reaction on a closed shell target plus one nucleon [Fras 89, Chom 86]. The formation of a GR state in a transfer reaction was mentioned by Olmer et al. [Olme 78]. But the experimental data were not enough to provide a convincing identification of the broad peaks observed in the transfer reactions as GR states.

Giant resonance states and single particle states have different properties, and it may be possible to distinguish between them. In GR excitations, the motion is highly collective and many particles in the nucleus are involved. The excitation energies of GR states change very smoothly with the mass of the nucleus. On the other hand, for single particle states, only a few particles are involved and the excitation energies of similar single particle states may change substantially even for neighboring nuclei. For a closed shell target, both proposed explanations lead to similar behavior, therefore it is difficult to distinguish between these two explanations by measurements on only

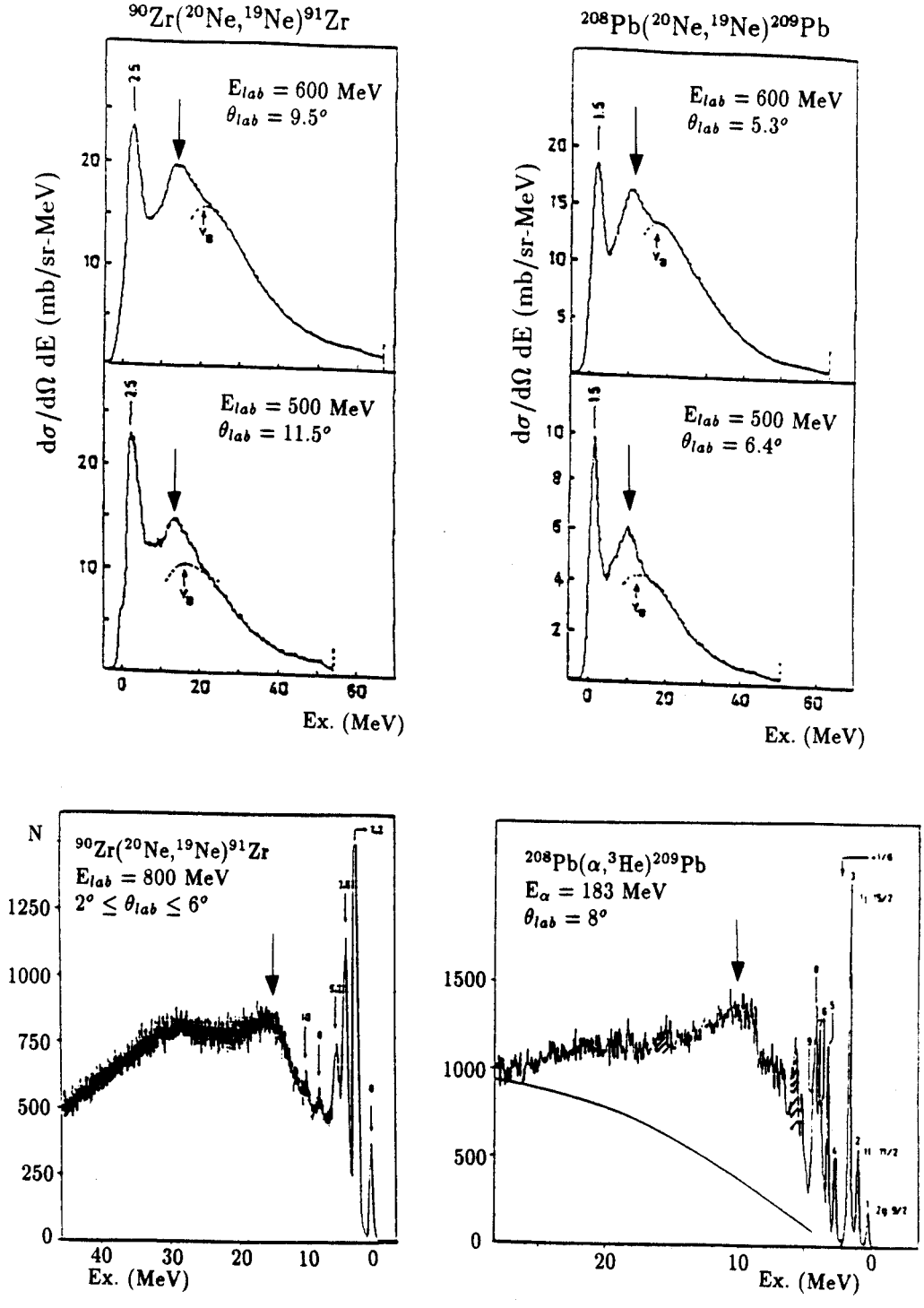

Figure 1.1: Broad peaks obtained by a neutron transfer reactions. The properties of the broad peaks (marked with arrows) are very similar to those of GR states [Fort 90, Fras 87, Mass 86].

closed shell targets. However, if the spectrum from a closed shell nucleus is compared with spectra from the same reaction for neighboring *even – odd* targets, one can distinguish the two models, because in this case one expects that the differences are large enough to be observable.

In this thesis, heavy ion transfer reactions have been investigated on even and odd A targets to try to resolve the question as to whether the broad peaks observed these reactions arise from GR excitation or from the excitation of single particle states. In addition, the underlying background observed in stripping reactions has been calculated using different models and the calculations have been compared to the experimental data.

1.2 Selection of Targets and Projectiles

The choice of targets was based on the following considerations. Consider a neutron stripping reaction on the *even – even* target ^{208}Pb leading to the residual nucleus ^{209}Pb. The low lying states formed in ^{209}Pb are the well known single neutron states which lie above the closed N=126 core. If the same reaction is carried out on the neighboring nucleus ^{209}Bi which has an extra $1h_{9/2}$ proton outside the Z=82 core, multiplets of states are formed from the coupling of the $1h_{9/2}$ proton with the aforementioned neutron states. These multiplets occur at about the same excitation energies in ^{210}Bi as the corresponding single neutron states in ^{209}Pb. However a different situation arises if a ^{207}Pb target is used. The ^{207}Pb nucleus has a $3p_{1/2}$ neutron hole state in the closed N=126 shell. Therefore the 0^+ ground state of ^{208}Pb is formed when a neutron is added to this hole. As a neutron is added to other higher lying neutron particle states, multiplets are produced due to the coupling of the $3p_{1/2}$ neutron hole with the neutron particle states. The excitation energies of these multiplets are

shifted to higher excitation approximately by the difference between the 0^+ ground state and the first multiplet. Such effects arise from rather general properties of single particle transfer reactions on neighboring nuclei. In contrast, the excitation energies of collective states like the GR change by much less than 0.1 MeV with a change of one in the mass of the target. Thus one may distinguish between collective and single particle states by measuring stripping reactions on ^{208}Pb, ^{209}Bi and ^{207}Pb. Similar behavior is expected for stripping reactions in the vicinity of closed shell target ^{90}Zr where one may perform a similar study using ^{90}Zr, ^{89}Y and ^{91}Zr targets.

Thus, reactions were measured for two *even – even* nuclei ^{208}Pb and ^{90}Zr and their neighboring nuclei, four *even – odd* nuclei ^{207}Pb, ^{209}Bi, ^{89}Y and ^{91}Zr as targets.

In choosing the projectiles, two conditions were considered. First, the ejectile excitations should be minimized to prevent the occurrence of spurious peaks in the spectrum from ejectile excitation. The problem of ejectile excitation may be reduced by using unbound or very weakly bound ejectiles such as *d*, ^{6}He, ^{6}Li, ^{8}Li and ^{13}N. Since the ejectiles excited above their "breakup threshold" decay into two or more fragments, they will not contaminate the spectrum at energies above this threshold. Second, the projectile energy should be high enough to excite the high lying states. However, as the projectile energy increases, the resolution becomes worse and the cross section for the breakup process increases faster with bombarding energy than the cross section for transfer reactions. To excite a high spin state, heavy ions are better than light ions, but the resolution is not as good as for light ions at the same projectile energy per nucleon. Thus, a compromise had to be made in choosing the projectiles and bombarding energies.

For the nucleon stripping reactions (^{7}Li,^{6}Li) and (^{7}Li,^{6}He), the projectile was chosen because the resultant ^{6}He and ^{6}Li ejectiles have threshold energies for breakup which are lower than the energies of their first excited states. In this case, one

expects ejectile excitation to be negligible. However projectile breakup still remains a dominant source of background at high excitation energies. The ^{7}Li beam is not suitable for measuring the proton pickup reaction (^{7}Li,^{8}Be), because ^{8}Be has a lifetime which is too short to be detected in the focal plane of the S320 spectrograph. Instead, the proton pickup reaction was measured with a ^{12}C beam, which again produces an ejectile ^{13}N for which the threshold energy for breakup is lower than the energy of the first excited state. For neutron pickup, both the (^{7}Li,^{8}Li) and (^{12}C,^{13}C) reactions were measured in order to estimate the contributions from ejectile excitation.

These reactions were measured at a projectile energy of 30 MeV/n because at this energy a large bump has already been seen in the ^{208}Pb(^{20}Ne,^{19}Ne) reaction [Fort 90].

1.3 Outline

In chapter 2, the experimental setup and procedures are described. These include the target preparation, detection system, electronics, and the method of calibration.

In chapter 3, shell model calculations useful for the description of one nucleon transfer reactions on ^{207}Pb and ^{209}Bi nuclei are presented. These calculations provide information on the energy levels of the multiplet states, such as the excitation energies, spectroscopic factors, and the shift of the centroid energy of the multiplets. The calculations are compared with the experimental data.

In chapter 4, the characteristics of the single particle states and GR states, and the method used to distinguish between the two states are described. The data obtained at the same kinematic conditions on *even – even* targets and *even – odd* targets for ^{90}Zr region and ^{208}Pb region are compared as a function of both the reaction Q – values and the excitation energies.

In chapter 5, the results for the one nucleon stripping reactions are presented. The

spectrum from the closed shell target nucleus is compared with the spectra from the neighboring targets. The relative strengths between the states are explained by the angular momentum transfer matching conditions. Evidence relevant to the nature of the broad peaks is presented.

In chapter 6, the background for the stripping reaction is described. Two theories for calculating the background: the Serber Model, and the Semi-Classical theory developed by Brink and Bonaccorso, are outlined and the corresponding calculations are compared with the experimental measurements. In addition, a test run for a coincidence measurement aimed at providing more information on the background is described.

In chapter 7, the results for the one nucleon pickup reactions are described. Ejectile excitation is shown to present significant problem for the interpretation of the neutron pickup reactions. The nature of the high lying peaks is discussed.

In chapter 8, a summary of this thesis and suggestions for future work are described briefly.

Chapter 2

Experimental Setup and Procedures

The transfer reactions (^{7}Li,^{6}Li), (^{7}Li,^{6}He), (^{7}Li,^{8}Li), (^{12}C,^{13}C) and (^{12}C,^{13}N) were carried out at a bombarding energy of 30 MeV/n using the K500 superconducting cyclotron at Michigan State University. The average beam current was between 10 and 20 particle nA (pnA). The targets used in this experiment, ^{89}Y, ^{90}Zr, ^{91}Zr, ^{207}Pb, ^{208}Pb and ^{209}Bi were all self supporting and had thicknesses of about 5 mg/cm^2. The thicknesses were chosen on the basis of the transfer reaction cross sections, counting rate, and the energy resolution for the given beams. The reaction products were analyzed with the S320 broad range magnetic spectrograph [S320 90] and detected by the focal plane detector system. In each reaction, the ejectiles were measured at the grazing angles to give large cross sections. The energy resolution was about 500 keV full width at half maximum (FWHM) for the ^{6}Li and ^{6}He spectra, and about 1 MeV FWHM for the ^{12}C, ^{13}C and ^{13}N spectra. In this chapter, the experimental equipment, procedures and analysis methods are described.

2.1 Target Preparations

Six targets, ^{89}Y (5.30 mg/cm^2, 100%), ^{90}Zr (5.06 mg/cm^2, 97.62%), ^{91}Zr (5.01 mg/cm^2, 88.5%), ^{207}Pb (4.95 mg/cm^2, 92.40%), ^{208}Pb (5.84 mg/cm^2, 99.14%) and ^{209}Bi (6.50 mg/cm^2, 100%) were used in this experiment. The ^{89}Y target was purchased from the Johnson Matthey Company. The original thickness of the yitrium target was 11.18 mg/cm^2 when it was purchased. A target of thickness, 5.3 mg/cm^2, was obtained by using a rolling machine. The thickness was determined by measuring the energy loss of α-particles emitted from an ^{241}Am source. The uniformity was $\pm$0.2 mg/cm^2 over the central region of the target. This method was verified by weighing the target. There was about a 10% difference between the two methods. This caused an uncertainty up to 10% in the absolute cross section.

The ^{209}Bi target was fabricated at Michigan State University using vacuum evaporation. When pure ^{209}Bi metal was heated in the furnace in a vacuum chamber, ^{209}Bi molecules evaporated and were deposited on a glass plate which was coated with detergent and placed about 15 cm above the ^{209}Bi source. The growth rate was dependent on the temperature of the furnace. The on-line measurement of the thickness of the target using a quartz crystal vibrator provided a rough indication of the thickness. The thickness was measured again after the target was floated off the glass slide. The exact thickness was obtained by measuring the energy loss of α-particles. The uniformity of the target was within $\pm$0.4 mg/cm^2.

The other targets, ^{90}Zr, ^{91}Zr, ^{207}Pb and ^{208}Pb were purchased from the Micro Matter Company. No noticeable sign of oxidation of the targets was observed in the data.

2.2 S320 Spectrograph

The reaction products were analyzed with the S320 magnetic spectrograph and charged particles were detected in a standard focal plane detector. This spectrograph has a K-parameter of 320, where K is defined by the equation $E/A = K(q/A)^2$, where E/A is the maximum allowable kinetic energy in Mev per nucleon, and q is the charge of a reaction product [S320 90]. The S320 spectrograph is designed to be operated in the dispersion matched mode. The kinematic effects due to the finite angular acceptance of the spectrograph are compensated by refocusing the quadrupole doublet according to the kinematic parameter of the reaction. The particles scattered from the target into a given solid angle and having the same momenta could be focused on the same position of the focal plane detector. The dynamic range in momentum covered by the spectrograph in a single setting is $\Delta P/P = 10\%$, the maximum solid angle is 0.67 msr and the angular range is from – 4 to 55 degrees. A schematic view of the S320 spectrograph is given in fig. 2.1 and some important parameters of the spectrograph are given in table. 2.1.

The S320 spectrograph is composed of a target chamber (or a scattering chamber), QQDMS (Quadrupole, Quadrupole, Dipole, Multipole (which is predominantly Octupole) and Sextupole) magnets and focal plane detectors. The target chamber is a precision scattering chamber with a sliding seal. The inner diameter is 39 cm and the inner height is 15 cm. The upper part of the chamber, including the lid, is braced to the wall and does not move. At the center, there is a target ladder with a circular platform. The target ladder can move up and down, and the ladder and the platform assembly may be rotated together independently of the spectrograph rotation. A total of 6 targets could be mounted in the target ladder at a same time. One target position was used for a scintillator of CsI crystal as a beam viewer. An-

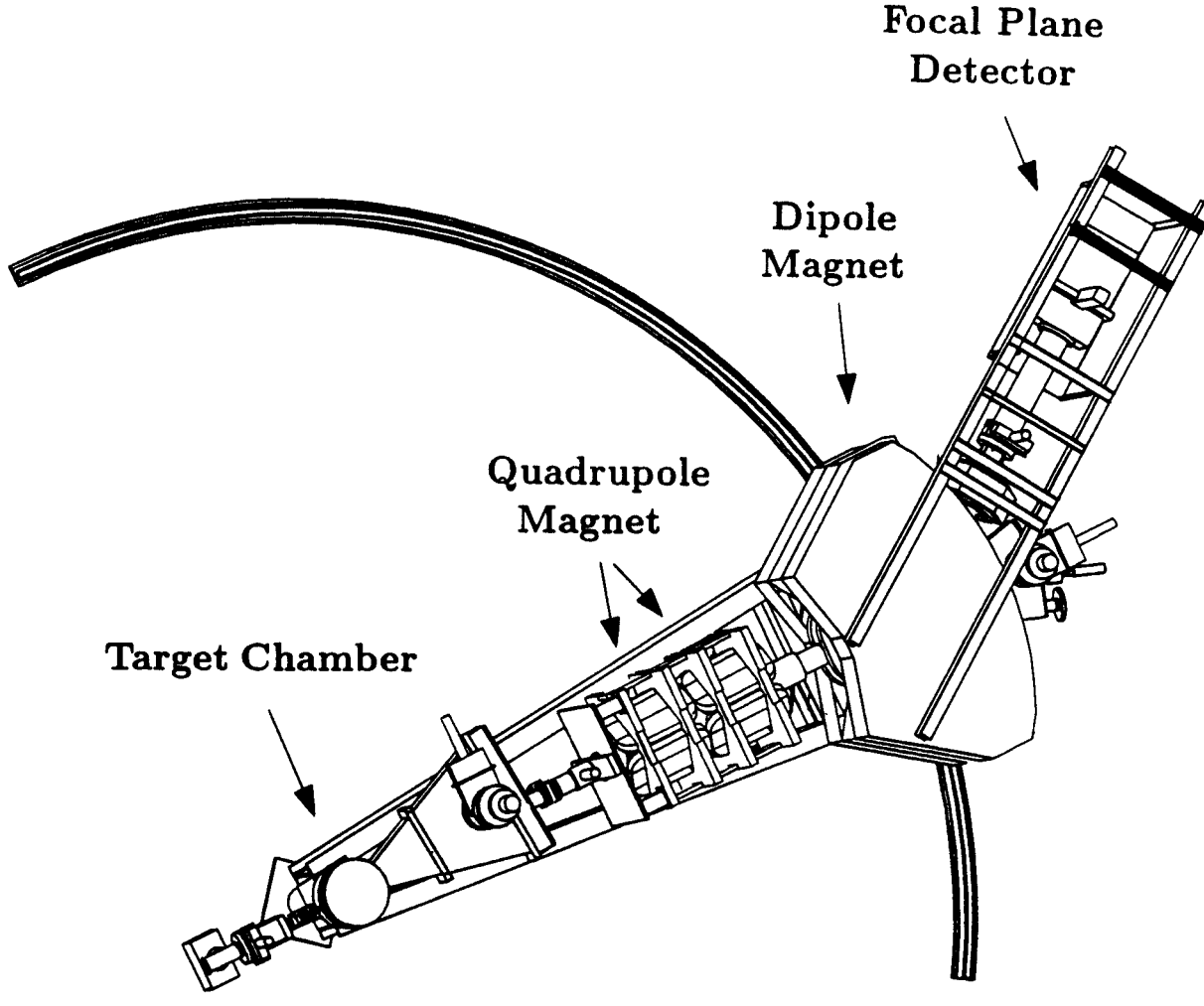

Figure 2.1: Schematic view of the S320 spectrograph.

Table 2.1: Parameters of the QQDMS S320 spectrograph.

Quad(Y) – Quad(X) – Dipole – Octupole – Sextupole	
Dispersion:	D = 1.6 cm/% ($\Delta p/p$)
Magnification:	Mx = −0.67 (D/M = 2.4)
	My = −2.5
Max. solid angle:	$\Delta\theta$ = 12 mr
	$\Delta\phi$ = 12 mr
	Ω = 0.67 msr
Beam spot on target (assumed):	
	0.5 mm incoherent width
	3 mm tall, dispersion matched
	2.4 mm dispersed beam width for 0.1% energy spread
Calculated line width (ray tracing):	
	$\Delta E/E$ = 0.1%, 0.8 mm
Range:	$(E_{max}-E_{min})/E$ = 20%
Focal plane:	Normal incidence, 18 cm long x 2.6 cm tall
Bend angle:	34.4°
Max rigidity:	$B\rho$ (max) = 2.57 T–m @ 1.47 T
	ρ (max) = 1.75 m
Central ray radius:	ρ (mean) = 1.70 m
Distance target → aperture:	1.965 m
Distance target → focal plane:	6.75 m
Distance target → scintillator:	7.12 m
Angular range:	−4° to 55°

other was used to hold a blank target to check the target frame contribution to the background, and a third one was used for a thin ^{12}C target for calibration. Therefore only three targets for reactions would be mounted at the same time in the ladder during the experiment. Two monitor detectors (bare photodiodes) were used. They were mounted on the lid of the chamber which is stationary and were located at a distance of 15 cm from the target. The distance between monitors was 1.5 inches and they were located at the lower left and lower right from the beam path. The aperture of the spectrograph is located at a distance of 196.5 cm from the target. Four different types of apertures, round holes of 8 mm and 25 mm diameter, a square 50 mm X 50 mm aperture and a 19 mm X 40 mm rectangular slit could be inserted remotely depending on the counting rate required.

There are two kinds of Faraday cups mounted in the S320 spectrograph. These cups stop the beam and accumulate the charge passing through the target. One is mounted in the wedge chamber for small angles, ranging from 1.5 to 9.5 degrees. The other one is mounted on the lid of the target chamber and is therefore independent of the spectrograph rotation. The minimum spectrometer angle such that this latter Faraday cup does not obscure the aperture is about $2.9 + W/2$ degrees, where W is the full opening angle of the spectrometer aperture. The biggest width of the aperture used in this experiment was 5 cm. In this case that W would be 1.46 degree and the minimum spectrometer angle possible would be 3.63 degree. Because the spectrometer angles used in the present experiments are 6 and 9 degrees, only the target chamber Faraday cup was used in this experiment.

The main role of the QQDMS magnet system is to separate the particles spatially on the focal plane where they are detected by a position sensitive detector according to the momentum and charge state of the particles. One of the quadrupole magnets focuses the particles in the Y – direction and the other one in the X – direction. The

dipole magnet bends the particles according to their magnetic rigidity $(B{\cdot}\rho = P/q)$, where P is the momentum and Q is the charge of the particle, B is the magnetic field and ρ is the orbit radius. The multipole and sextupole magnets are used to help focus the particles at the focal plane of the detector and to minimize the aberrations.

2.3 Focal Plane Detectors

The focal plane detection system of the S320 spectrograph is composed of three modular units: position sensitive counters, ion chambers, and scintillators. A schematic view of the detector system is given in fig. 2.2. A position sensitive single wire proportional counter (SWPC) is followed by two ionization chambers (IC), then another SWPC and scintillator (SCNT). All the gas detectors operate with the same gas volume and thus have the same pressures and are separated from the spectrometer vacuum by a Kapton window of thickness 25 microns which can hold a pressure difference of one atmosphere. Depending on the charges and the energies of the reaction products, different types of gases and pressures were used. For the ^{12}C beam, 100% isobutane gas was used at 70 torr, and for the ^{7}Li beam, a mixture of 20% of isobutane gas and 80% of freon gas was used at 140 torr. The mixed gas does not have as large a gain as the pure isobutane gas. However the uniformity in the mixed gas is better than that of pure Isobutane gas and less sensitive to poisoning. With the ^{7}Li beams, because there was no difficulty in particle identification, the mixed gas was used for better uniformity.

The SWPC detector enables one to obtain the position spectra using the charge division method (the relative ratio of the pulse heights from the two ends of the resistive wire). For precision measurement of the particle position, the gains of the amplifiers (front wire left and front wire right, back wire left and back wire right)

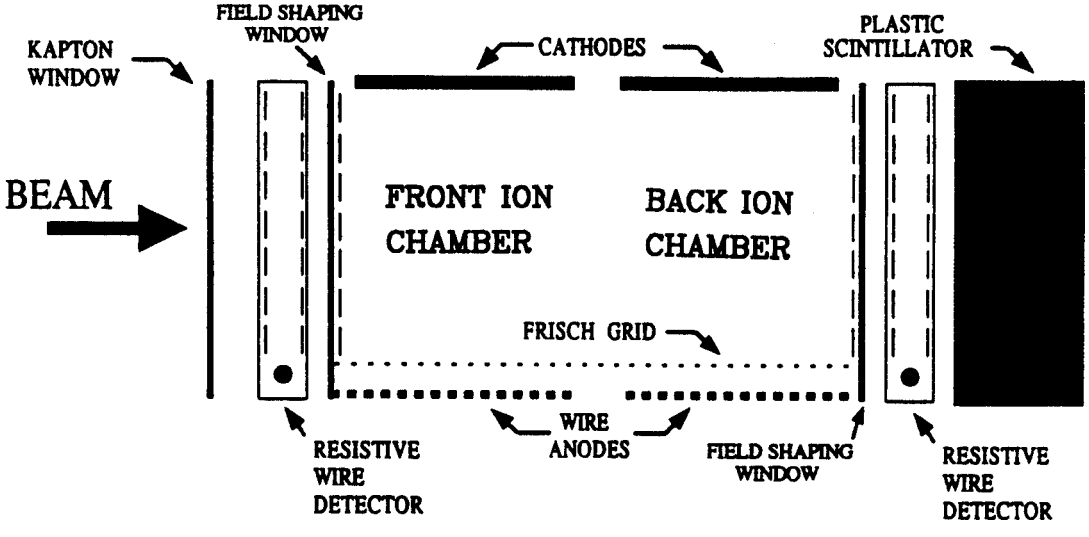

Figure 2.2: Schematic view of the focal plane detector [Moha 91].

were matched using a test signal. Adjustments for all the other amplifiers were also done before taking the data and the initial settings were not changed until the end of the experiment. A stopping scintillator is mounted behind the gas detectors. This is composed of a thin (0.51 mm) fast scintillator and thick (10 cm) slow scintillator. The output signal is the sum of the fast and slow scintillator signals and this signal was used as a start signal. The time of flight of the particles was obtained by measuring the difference between the cyclotron RF and the scintillator signal.

2.4 Electronics

The electronics used for the data taking is displayed in fig. 2.3. The same electronic setup is used for most experiments with the S320 spectrograph. Ten signals were obtained from the various detecting modules and were recorded after they were processed by the electronics. A S320 spectrograph event was normally defined by the total scintillator signal (fast + slow) above a constant fraction discriminator (CFD) level. The signals from the scintillator left and scintillator right passed through the coincidence checking circuit. When the two signals were above a CFD level and coincident, a true event was assumed and the output signal from the coincidence checking circuit was used as a start signal (or a S320 master signal). This signal was used to open the gates of the ADC and QDC modules, and as a start input of the TDC and the TAC. The signals detected from the two wire counters, two ion chambers and two monitors were digitized with an ORTEC AD811 analog to digital converter (ADC) and the signals obtained from the scintillator were digitized with a LECROY 2249W charge to digital converter (QDC). From the left and right signals from each wire counter, the position was calculated, and the difference between the two detected positions of the wires was used to measure the scattering angle relative to the central angle of the spectrograph. The TDC signals were used for the time of flight

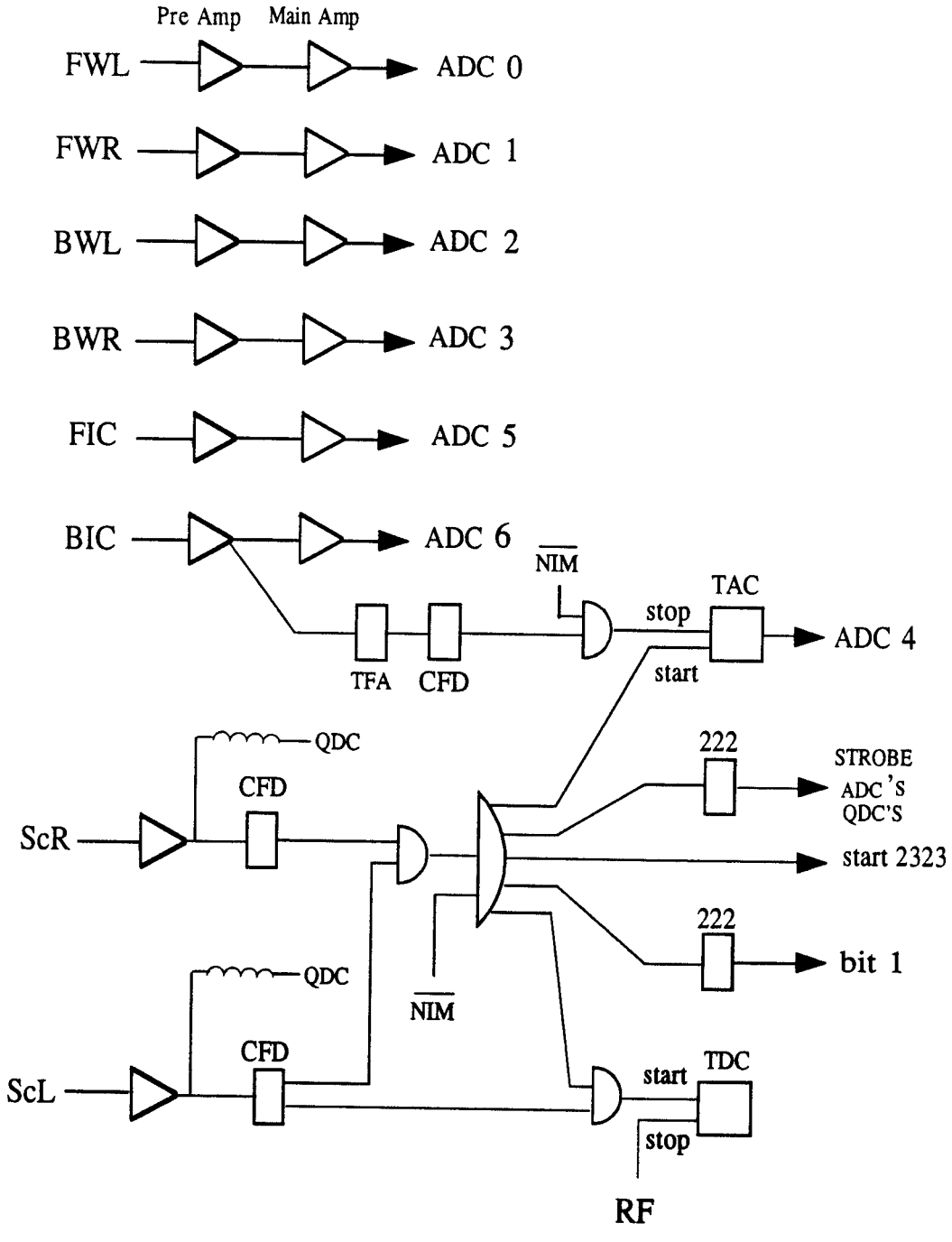

Figure 2.3: Schematic view of the S320 electronics [S320 90].

(TOF) information. For the TOF relative to the cyclotron RF, the TDC was started by either the left or the right scintillator delayed CFD output and was stopped by the cyclotron RF signal. A time to pulse height converter (TAC) signal was used to find the vertical position in the front ion chamber by measuring the drift time of the electrons. The TAC was started by the S320 master signal and stopped by one of the front ion chamber signals. The TAC signal was read by an ADC.

The signals which were digitized by ADC, QDC or TDC were recorded by the program ROUTER in the VME bus front ends based on multiple MC680x0 architecture processors as part of CAMAC data acquisition system [Fox 85, Fox 89, Sher 85]. The flow diagram of the data taking system is given in figs. 2.4 and 2.5 [Winf 91]. This system blocks the recorded events into 8192 byte buffers and then sends them back to the VAX/VMS system for on-line event recording and analysis. The buffered data are read by the program ROUTER and sent to specified subprocesses. There are three main subprocesses. One is a scaler display task which sums and displays scaler totals, and another is a tape writing task which writes the data buffers to tape. The other one is a data analyzing program, SARA [Sara 90], which identifies the particles and creates displays on the terminal. During the experiment, a fraction of the total data was displayed on the terminal and analyzed on-line as a check on the progress of the experiment.

2.5 Magnetic Field Setting

There are five magnets (QQDMS) which need to to be set to focus the particles on the focal plane. The functions of these magnets were described in section 2.2. The values for the field settings were obtained by executing the program *nscl_library* : [*setup.s*320]*s*320.*exe* with the inputs such as reaction formula, lab. angle, energy/n

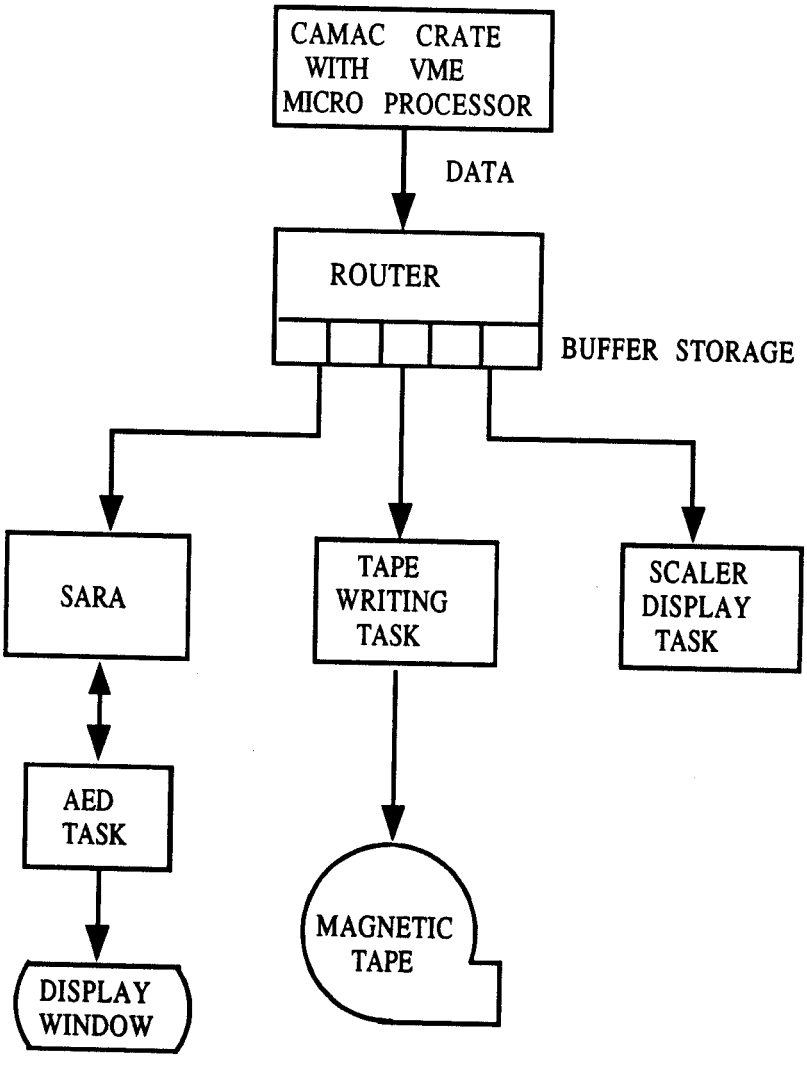

Figure 2.4: Flow diagram of on-line data taking system [Winf 91].

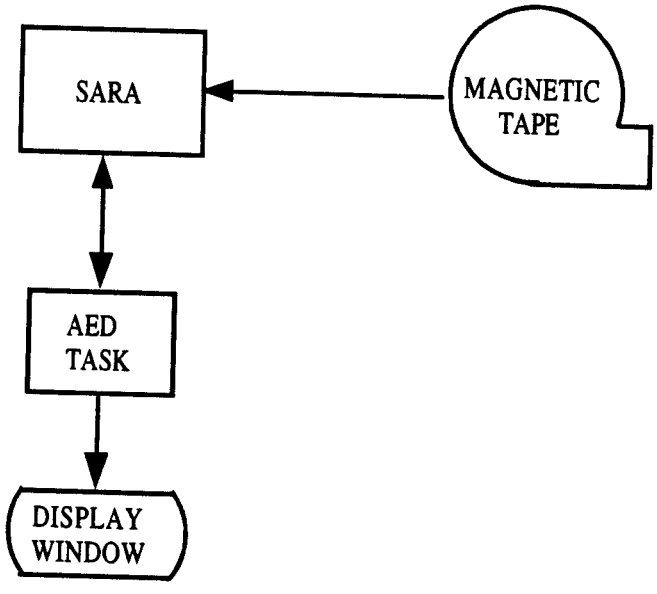

Figure 2.5: Flow diagram for off-line data taking system. [Winf 91]

and excitation energy of the residual nucleus. This program calculates the kinetic energies of the reaction products, magnetic fields of 5 magnets, grazing angles, C.M. angles for the given lab angles and time of flight. The masses of the particles were taken from the mass table of nscl_library : [mass86] mass86obj/lib. The magnetic fields were calculated with fully relativistic kinematics and were based on empirical calibrations. For each reaction, the fields were reset because of the different kinematics. The dipole field was measured with the SENTEC NMR system. When the dipole field strength was higher than 14 *kGauss* as was the case for the (^{7}Li,^{6}He) reaction, the field measured by the NMR probe was not very stable.

The calculated field settings focus the highest energy particles of interest on the middle of the focal plane single wire proportional counter (SWPC).

2.6 Particle Identification

The particle identification was done using the program *SARA* which allows gate and contour setting, and histogramming with or without conditions [Sara 90]. The gates can be set on the AED terminal by marking two points on a one dimensional histogram or by drawing a contour on a two dimensional plot which is composed of two parameters out of energy loss in ion chamber (ΔE), light out of scintillator (E), time of flight (TOF), and position in the focal plane (POS). The ion chamber was filled with a mixed gas of freon (80%) and isobutane (20%) at a pressure of 140 torr for the ^{7}Li beam and 100% isobutane gas at pressure of 70 torr for the ^{12}C beam. The energy loss in this chamber is proportional to Z^2/v^2, where Z is the charge state and v the velocity of a detected particle. The particles separate cleanly when Z is different at a similar energy per nucleon. TOF is proportional to M/Z where M is a mass of a particle. This permits good separation of a particle which has a different

mass from particles which have the same charge states. The program *SARA* was used for both on-line and off-line data analysis. In the on-line analysis, this program was used to display a sample of the collected data on the AED terminal. By setting the gates or contours on the spectra of the terminal while taking the data, spectra of specific reaction products could be checked to see if the data acquisition process was working correctly. In most of the reactions, two contours were used on the two dimensional spectra of $\Delta E.vs.E$ and $TOF.vs.POS$.

In the off-line analysis, clearer particle identification was possible. In the (^{7}Li,^{6}Li) reactions, because any single contour was not enough to separate ^{6}Li particles clearly, two contours on the $\Delta E.vs.E$ and $TOF.vs.POS$ spectra were used. The particles of charge state 3 were separated using the $\Delta E.vs.E$ spectrum and ^{6}Li particles were separated using the $TOF.vs.POS$ spectrum.

In the (^{7}Li,^{6}He) reactions, only ^{6}He, and ^3H which came from the direct breakup of ^{7}Li$\rightarrow^4$He + ^{3}H were detected. Because of big differences of Z^2/v^2 between the two particles, ^{6}He particles were cleanly separated in the $\Delta E.vs.E$ spectrum.

In the (^{12}C,^{13}C) reactions, because the magnetic rigidity (P/q) of ^{13}C is not much different from that of ^{12}C, the elastically scattered ^{12}C particles were also detected at the focal plane corresponding to excitation energies of about 25 MeV in the residual nuclei. Because the counting rate of elastically scattered ^{12}C particles was much larger than ^{13}C particles, the ^{12}C particles were blocked by using a "finger". The particle identification was done with two contours on the $\Delta E.vs.E$ and $TOF.vs.POS$ spectra.

In the (^{12}C,^{13}N) reactions, elastically scattered ^{12}C particles did not disturb the detection of ^{13}N particles and no blocking finger was used. The particle identification was done with the same method as for the ^{13}C particles. Some typical two dimensional spectra and contours for particle identifications are shown in fig. 2.6

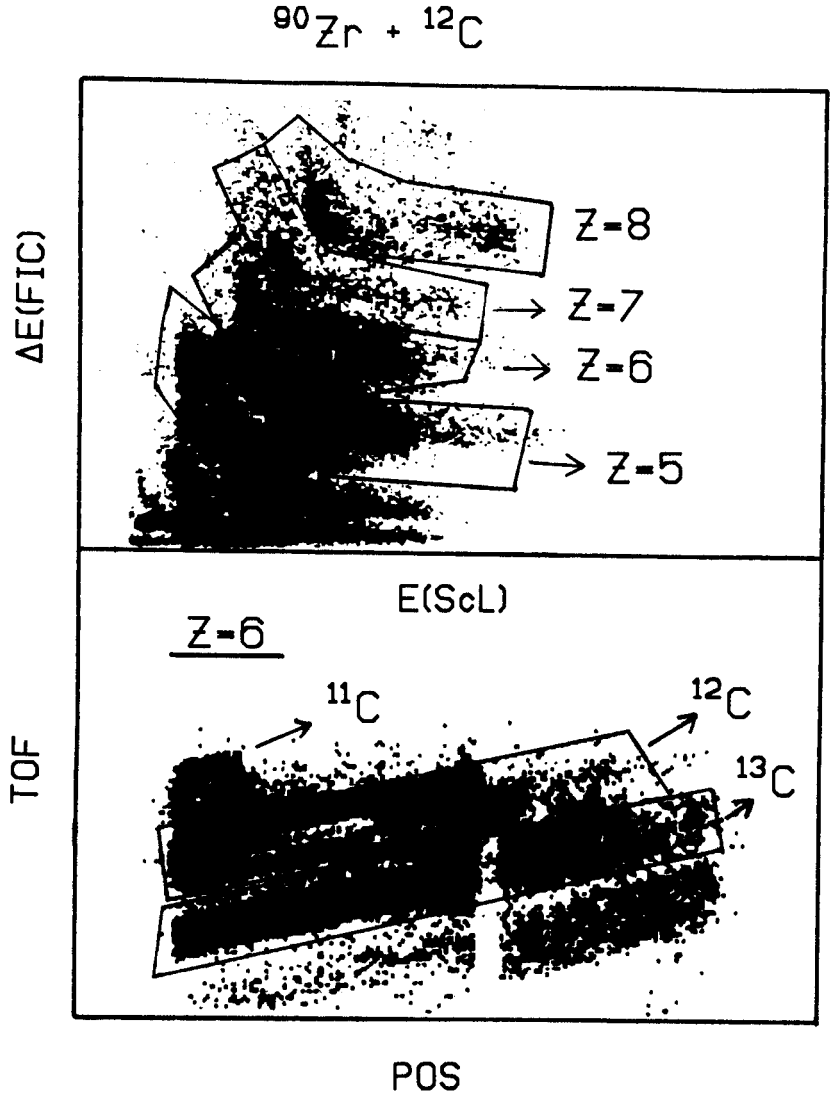

Figure 2.6: A sample of particle identification in two dimensional spectra for ^{90}Zr + ^{12}C reaction.

2.7 Energy Calibration

Energy calibration enables one to find the relation between the energies and the channel numbers of various particles detected in the focal plane detector. From magnetic rigidity, $B \cdot \rho = P/q$, the orbit radius ρ in a known magnetic dipole field B can be calculated for a detected particle of momentum P and charge state q. The orbit radius may be expressed in terms of a channel number using a simple polynomial of specified order. Normally a second order polynomial is sufficient. Then the relation between the calculated orbit radius ρ and the measured channel number x is given as

$$\rho = a + b \cdot x + c \cdot x^2. \tag{2.1}$$

To obtain the coefficients a, b and c at least 3 different settings of B and x are required. For the calibrations of this experiment, channel number x was obtained by changing the magnetic field B, with the same target at a fixed scattering angle. Once the calibration is done for a specified particle, the momentum and the related physical quantities can be extracted from the measured channel number, and this calibration may be applied to calibrations of energy spectra for other particles which have similar mass and energy. The calibration obtained for the ^{6}Li spectra may be applied to the calibration of ^{6}He or ^{8}Li spectra, but may not be acceptable for the calibration of ^{13}C or ^{13}N spectra because of the big differences in energies and momenta, and the nonlineality of the energy calibrations.

In this experiment, the ^{6}Li and ^{6}He spectra were calibrated using the reactions ^{12}C(^{7}Li,^{6}Li) and ^{12}C(^{7}Li,^{6}He). To minimize the uncertainty in the calibration due to the energy loss in the target, a very thin ^{12}C target (0.48 mg/cm^2) was used. For calibrations of ^{13}C and ^{13}N spectra, ^{12}C spectra on a target of ^{90}Zr of thickness 5.3 mg/cm^2 were used with elastic scattering reactions. The reason that ^{12}C spectra were

used instead of ^{13}C or ^{13}N spectra is that the ground state of ^{89}Zr or ^{89}Y was not separated cleanly from the excited states. The calibration coefficients were obtained by executing the program $NSCL\_LIBRARY : [SETUP.CALLIB]CAL88.EXE$. A detailed description is given in ref.[S320 90]. The fitted calibration curves for the ^{6}Li, ^{6}He and ^{12}C spectra are given in fig. 2.7.

The relativistic momentum P can be calculated for a given reaction, with known x, B and q. Then it is possible to predict the location or the channel number of a known state, or determine the excitation energy, reaction Q – value and particle's kinetic energy for a given channel number. To find the excitation energy corresponding to the ejectile's kinetic energy some relativistic kinematics are required. A diagram depicting the initial, intermediate, and final systems involved in the kinematics of transfer nuclear reaction is given in fig. 2.8. E_n, M_n and P_n are kinetic energy, mass and momentum of the n^{th} particle just before and after the reaction. It is assumed that the reaction happened at the middle of the target. As the particle's momentum and the position are measured after the reaction using the S320 spectrograph, it is necessary to compensate for the energy loss in the target. Thus the final form for the residual nucleus's excitation should be expressed in terms of the initial and final system's known parameters. The x and y – components of the momentum must be conserved, i.e.

$$P_1 = P_3 \cdot \cos\theta + P_4 \cdot \cos\psi, \tag{2.2}$$

$$P_3 \cdot \sin\theta = P_4 \cdot \sin\psi. \tag{2.3}$$

By eliminating the term which has ψ,

$$P_4^2 = P_1^2 + P_3^2 - 2P_1 \cdot P_3 \cdot \cos\theta, \tag{2.4}$$

$$P_1 = \sqrt{E_1^2 + 2M_1 \cdot E_1}, \tag{2.5}$$

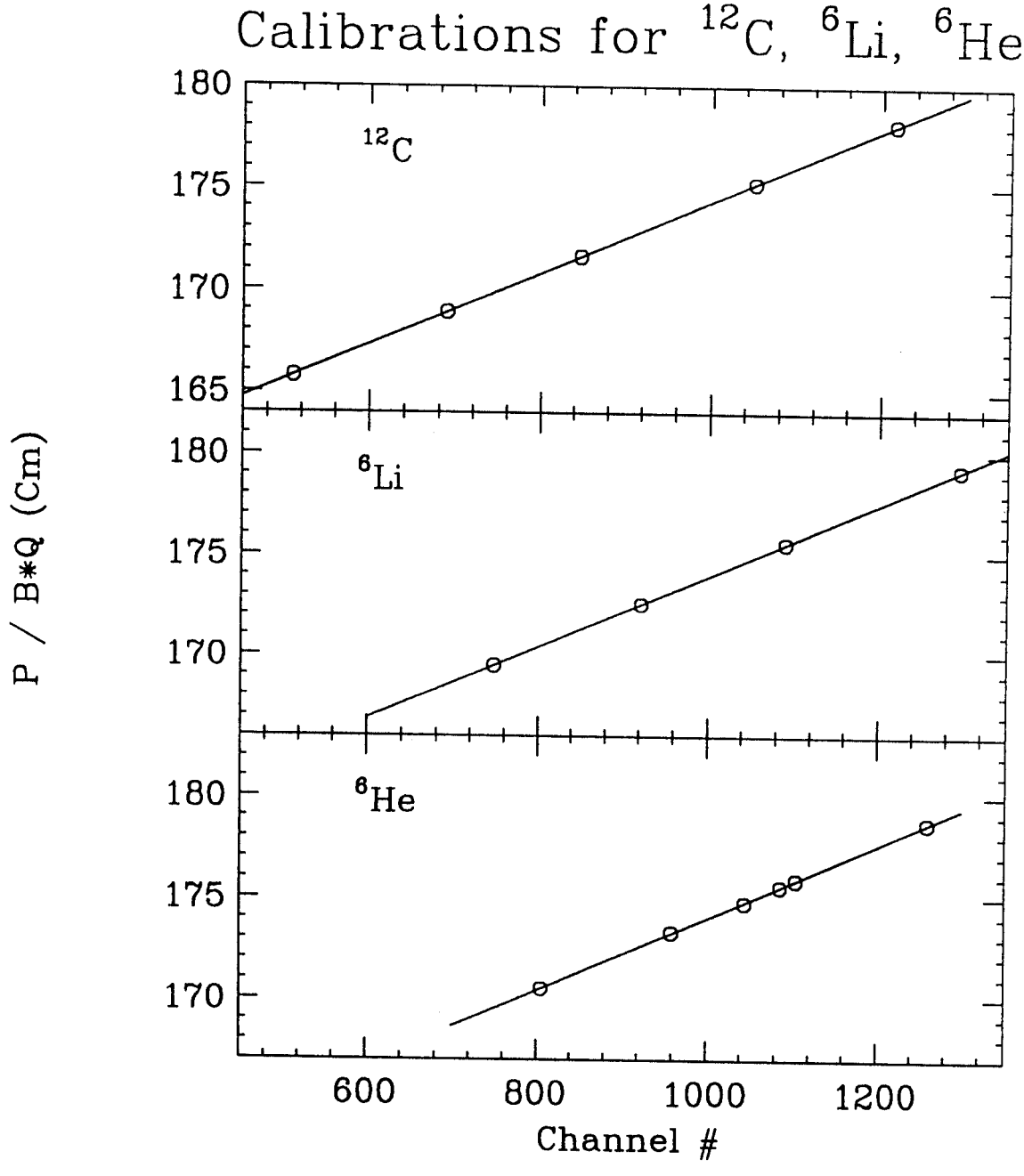

Figure 2.7: Calibrations on ^{12}C, ^{6}Li and ^{6}He particles. Uncertainty is about 0.1%.

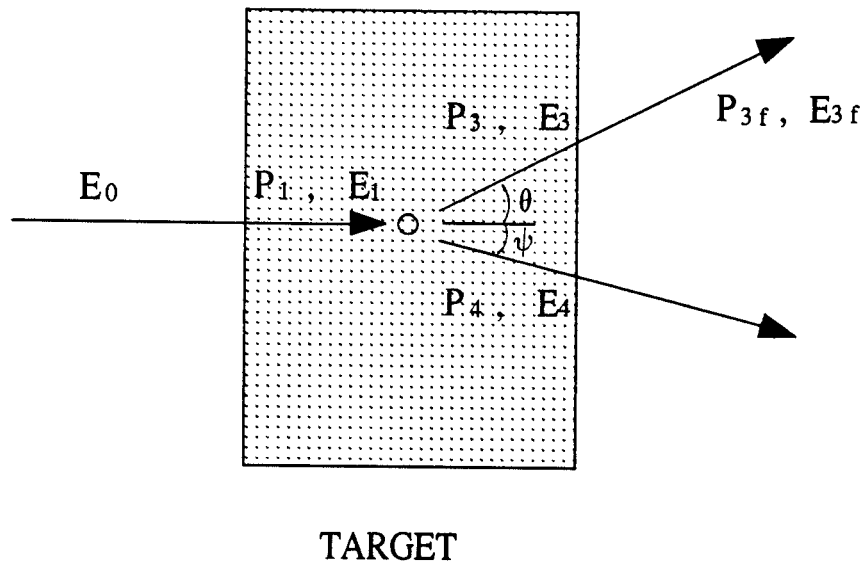

Figure 2.8: Schematic diagram depicting the kinematics in the target.

where $E_1 = E_0 - E_{lossin}$ and P_3 can be calculated easily using the measured channel number (ρ), E_{lossin}, $E_{lossout}$ and P_{3f},

$$P_{3f} = B \cdot \rho \cdot q/3.3356, \tag{2.6}$$

$$E_3 = E_{3f} + E_{lossout}$$

$$= \sqrt{P_{3f}^2 + M_3^2} - M_3 + E_{lossout}, \tag{2.7}$$

$$P_3 = \sqrt{{E_3}^2 + 2M_3 \cdot E_3}, \tag{2.8}$$

where momenta are expressed in a convenient unit (MeV/c) rather than an MKS unit, B is the magnetic field strength in kG, q is the charge state and ρ is the orbit radius in cm. E_{lossin} and $E_{lossout}$ are the incident particle and ejectile's energy loss in the first half and second half of the target. Now P_4 can be calculated from eq.2.4 by using P_1, P_3 and the scattering angle θ. The recoil energy is,

$$E_4 = \sqrt{P_4^2 + M_4^2} - M_4. \tag{2.9}$$

Then the excitation energy of the residual nucleus is

$$E_{ex} = E_0 - E_{3f} - E_4 + Q - E_{loss}, \tag{2.10}$$

where Q is a reaction Q – value and E_{loss} is the total energy loss in the target, sum of E_{lossin} and $E_{lossout}$. The energy losses in the targets were calculated by executing the program *nscl_library* : [*setup.eloss*]*donna.exe*. This program calculates the energy loss of any particles in any medium or series of media. The input parameters are, incident energy, proton number and nuclear mass of the projectile, and electron number, atomic mass, mass density and thickness of the target particles. In heavy targets, most of the energy loss is caused by inelastic collisions between the projectile and the atomic electrons of the target making an ionization or excitation of the target atoms. To determine the E_{lossin} and $E_{lossout}$, it was assumed that the reaction happened at the middle of the target. E_{lossin} is the energy loss of the projectile for the one half thickness of the target and $E_{lossout}$ is the energy loss of the ejectile for the other half thickness of the target. E_{lossin} is independent of residual nucleus's excitation, but $E_{lossout}$ is, because the kinetic energy of the ejectile, dependent on the excitation of the residual nucleus. In case when the residual nucleus was in an excited state after the reaction, $E_{lossout}$ was adjusted using the linear relation between the two cases of energy losses at $E = 0$ MeV and $E = 60$ MeV of a residual nucleus. Of course the exact excitation is not known in this step. But a small difference in excitation energy does not affect $E_{lossout}$ very much. If the excitation of the residual nucleus is E, then

$$E_{lossout,Ex=E} = E_{lossout,Ex=0.} + \frac{E}{60} \cdot (E_{lossout,Ex=60.} - E_{lossout,Ex=0.}). \qquad (2.11)$$

When the residual nucleus is in an excited state, the reaction Q – value is the sum of the excitation energy E and the reaction Q – value for the ground state of the residual nucleus,

$$Q = E + Q_{Ex=0.} . \qquad (2.12)$$

The calculated energy losses in the targets for the projectiles and the reaction products are given in table. 2.2.

Table 2.2: Energy losses of the reaction products in the targets at $E = 30$ MeV/n. Units are MeV. Numbers in parenthesis are target's thicknesses in mg/cm^2. Reac.Pro. represents "Reaction Products". Uncertainty is about 10%.

Target / Reac.Pro.	^{90}Zr (5.06)	^{91}Zr (5.01)	^{89}Y (5.30)	^{208}Pb (5.84)	^{209}Bi (6.50)	^{207}Pb (4.95)
^{7}Li	0.493	0.493	0.512	0.422	0.472	0.359
^{6}Li	0.440	0.437	0.457	0.382	0.426	0.322
^{6}He	0.199	0.198	0.204	0.172	0.191	0.146
^{12}C	1.976	1.973	2.052	1.690	1.888	1.439
^{13}C	2.134	2.109	2.214	1.800	2.012	1.531
^{13}N	2.903	2.900	3.006	2.467	2.736	2.099

The uncertainty of the calibration is about 0.15 MeV for ^{6}Li and ^{6}He, and about 0.3 MeV for ^{13}C and ^{13}N. The main uncertainties are from the inaccurate thickness of the target and the intrinsic uncertainty of the focal plane detecting system of S320 spectrograph. The final determination of the excitation energies was made by subtraction from the energy of the ground state which was set at $Ex. = 0$ MeV. The shifts to make $Ex. = 0.$ were less than 0.3 MeV for ^{6}Li and ^{6}He, and less than 0.5 MeV for ^{13}C and ^{13}N.

2.8 Cross Section Determination

The differential cross sections for the single nucleon transfer reactions were obtained by using the parameters measured in the laboratory frame. The formula used is

$$\frac{d\sigma}{d\Omega} = \frac{N_{spec}}{3.74 \cdot 10^{3}} \cdot \frac{Z \cdot m_t}{Q \cdot T} \cdot \frac{DTC}{\Delta\Omega}, \tag{2.13}$$

where N_{spec} is the number of the reaction products detected by the spectrograph per channel number, Z is the average charge number of the projectile after it passed through the target, Q is the integrated beam current in nC, m_t is the mass of the target nucleus in amu, T is the thickness of the target in mg/cm^2, $\Delta\Omega$ is the solid angle of the aperture in msr and DTC is the dead time correction coefficient. The cross sections are in mb/sr. The uncertainty for the cross section appears to be about 10% due to the the uncertainty of the target's thickness.

Chapter 3

Shell Model Analysis for ^{208}Pb Region Nuclei

3.1 Introduction

In single nucleon transfer reactions on targets which have an extra hole or particle outside a closed shell nucleus, the interaction between the transferred nucleon and the target's hole or particle is the main factor that splits the single particle states and produces a multiplet of states. At low excitation energies, the shift in excitation energy and a slight broadening of the peak due to this interaction were observed and discussed extensively on lead region nuclei using light ion transfer reactions [Alfo 70, Craw 73]. But at high excitation energies, the density of states is so high that individual states are not resolved. If the changes in excitation energies and widths of the multiplets due to the presence of an extra particle or hole can be predicted by theoretical methods, it would give us confidence in predicting the shifts in excitation energies at high excitation energy. One of the methods to calculate these changes is the shell model. This calculation provides us very useful information on the splitting of energy levels due to an extra particle or hole state, including the spectroscopic factors and the excitation energies by solving the Schrodinger equations for the given conditions assuming that nucleons inside the core nucleus are in the same average potential. From

this information, the shift and the broadening of the multiplet states from the single particle or single hole states can be obtained.

Shell model calculations have been very successful in the vicinity of the closed shell nuclei, especially in the lead region nuclei [Ma 73, Herl 72, Mcgr 75, Warb 91]. One problem with the shell model calculation is that there are many low lying single particle orbits which are potentially important. Thus very large matrices need to be diagonalized which requires too large a working area and cpu time for the available computers. Thus the number of particle states and hole states must be limited in these calculations.

For the chosen two target nuclei, ^{207}Pb and ^{209}Bi which have an extra single particle or hole outside the closed shell core nucleus ^{208}Pb, the energy levels and spectroscopic factors for the single nucleon stripping reactions were calculated. The purpose of the shell model calculation is to observe how the characteristics of the single particle states in the multiplet, such as excitation energies and spectroscopic factors, are changed by the presence of a single particle or hole outside a closed shell nucleus. But the single particle states at high excitation energies are not well known and it is therefore difficult to calculate the changes for the high lying particle states. But by calculating the changes for low lying particle states which are known well, one can assume that the results are applicable to high lying single particle states, since the interactions between the $p-p$ or $p-h$ states are not very dependent on the excitation energies.

3.2 Energy Level Calculations

For the single nucleon stripping reactions on targets of ^{207}Pb and ^{209}Bi, the energy levels, and their parameters such as excitation energies, wave functions and spectroscopic

factors were calculated using the NSCL version of the program OXBASH[OXBA 88]. This can handle up to 3 particle orbits and 4 hole orbits in both proton and neutron shells. The targets were assumed to be a composite of the ^{208}Pb core nucleus and a single proton particle for the ^{209}Bi nucleus or a single neutron hole for the ^{207}Pb nucleus. Energetically the highest 4 hole orbits and the lowest 3 particle orbits were considered to be the available particle and hole states both for proton and neutron shells. The experimental single particle energy levels in ^{208}Pb are given in fig. 3.1 [Ma 73]. (*proton particle* ; $1h_{9/2}, 2f_{7/2}$, $1i_{13/2}$, *proton hole* ; $1h_{11/2}, 3s_{1/2}$, $2d_{3/2}, 2d_{5/2}$, *neutron particle* ; $2g_{9/2}, 1i_{11/2}$, $1j_{15/2}$, *neutron hole* ; $1i_{13/2}, 3p_{1/2}$, $3p_{3/2}, 2f_{5/2}$)

The matrix elements of the Hamiltonian operator H between the many particle basis functions were obtained by using the second quantized operators a^+ and a [OXBA 88]. The Hamiltonian H can be written as

$$H = H_{core} + \sum_i \epsilon_i a_i^+ a_i + \sum_{i>j,k>l} v_{ijkl} a_i^+ a_j^+ a_k a_l, \tag{3.1}$$

where ϵ_i is the energy of a single particle state, and

$$v_{ijkl} = \langle ij|V|kl\rangle, \tag{3.2}$$

and $|ij\rangle$ is an antisymmetrized two particle m-scheme state. The values for the both ϵ_i and v_{ijkl} are inputs in the code OXBASH. The single particle energies ϵ_i are adjusted to fit the experiment and the two body terms v_{ijkl} were based on the Kuo-Herling G-matrix [Warb 91]. By applying this Hamiltonian operator to the wave function $|ij\rangle$ and diagonalizing the matrix elements, the eigenvalues and eigenfunctions can be obtained. Here, the eigenvalues are the energies of the final states.

In the ^{207}Pb$(+n)$ reaction, when the transferred neutron occupies one of the 3 neutron particle states, the neutron hole which is initially in the $3p_{1/2}$ state can be

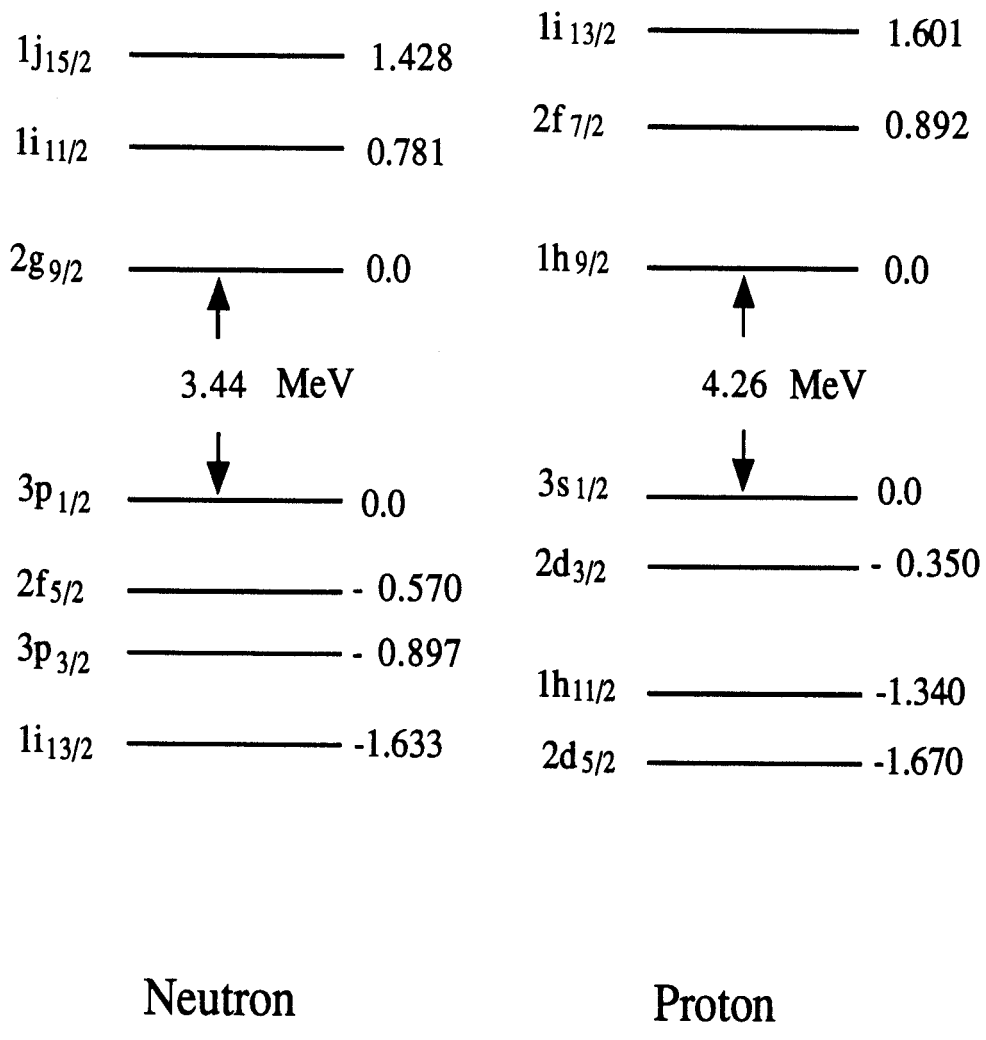

Figure 3.1: Experimental single particle and hole energy levels in ^{208}Pb [Ma 73]. In shell model calculation, the lowest 3 particle states and the highest 4 hole states for both proton and neutron shells were used.

located in any one of the 4 neutron hole states in the final state while the proton shell was assumed to remain closed. (The notation $(+n)$ stands for adding a neutron to the target by a neutron stripping reaction). So 12 combinations of one particle – one hole states were used in the calculations. If the neutron occupies the target's initial hole state $3p\frac{1}{2}^{-1}$, the neutron shell becomes a closed shell. In this case the proton shell was assumed either to be a closed shell or a proton can be excited to one of the 3 proton particle states from one of the proton hole states, which makes 13 (1+12) combinations. Thus a total of 25 combinations of particle and hole states were considered. Each combination has many different states due to the $p-h$ couplings.

The same procedures were also used for the other reactions. In the ^{209}Bi$(+n)$ reaction, since the target nucleus has a proton in the $1h_{9/2}$ orbit, the main interaction is between the transferred neutron and an outmost shell's proton. Three particle states are available for both proton and neutron shells, thus 9 combinations are allowed. In the ^{207}Pb$(+p)$ reaction, three proton particle states and 4 neutron hole states are available, thus total 12 combinations are allowed, where $(+p)$ represents adding a proton to the target by a stripping reaction. The main interaction comes from the coupling of the transferred proton and the target's neutron hole state. In the ^{209}Bi$(+p)$ reaction, there are two protons in proton particle states outside the closed ^{208}Pb core nucleus. A total of 9 combinations are possible.

3.3 Results and Discussions

The results for the energy levels are expressed as an excitation energy, spectroscopic factor S, j^π of the residual nucleus and a transferred nucleon's final orbit quantum numbers n, l and j. The cross section σ_f is defined as

$$\sigma_f = \sigma_{th} \cdot \frac{2J_f+1}{2J_i+1} S_f, \tag{3.3}$$

where σ_{th} is the cross section calculated theoretically and may be assumed to be constant for the same orbit. j_f and j_i are the total angular momentum of the final and initial state respectively, and S_f is the spectroscopic factor of the final state. The single particle states in the ^{209}Pb and ^{209}Bi nuclei are independently normalized to the experimental data, and the energy levels of each multiplet are plotted as a function of excitation energy after the strengths are normalized to those of the single particle states in the ^{209}Pb and ^{209}Bi nuclei (fig. 3.2). The average energies of each multiplet are obtained by averaging the energies weighted by the cross section. They are compared with the present experimental data, and the centroid energies are compared with the single particle states of the ^{209}Pb and ^{209}Bi nuclei in tables. 3.1 and 3.2, and fig. 3.3.

In the ^{207}Pb$(+n)$ reaction, the energy levels except the ground state are shifted to higher excitation, which agrees very well with the experimental result. The ground state is formed when a transferred neutron fills a target's hole, $3p_{1/2}$ state. As the final state is doubly closed, the shift of the ground state to lower energy (3.564 MeV) is much larger than in the $odd - odd$ (^{207}Pb$(+p)$ or ^{209}Bi$(+n)$) or non - closed $even - even$ (^{209}Bi$(+p)$) residual nuclei's ground states. The couplings between the neutron's particle state j^{π} and the ground state $3p_{\frac{1}{2}}^{-1}$ allow only two j_f of $j + \frac{1}{2}$ and $j - \frac{1}{2}$. Thus each multiplet is dominated by these two levels out of numerous levels which are not seen in the figure due to the very weak spectroscopic strengths.

In the ^{209}Bi$(+n)$ reaction, each multiplet is represented by many levels which have similar spectroscopic strengths, and the widths of the multiplets (about 500 keV) are somewhat bigger than those ($100 \sim 300$ keV) of the multiplets in the ^{207}Pb$(+n)$ reaction. The reason is that the ground state of ^{209}Bi, has a large angular momentum ($1h_{9/2}$) and the coupling with the neutron particle states allows many j_f ranging from $|j - \frac{9}{2}|$ to $j + \frac{9}{2}$. But the ground state is not shifted much (about 0.35 MeV) from

Figure 3.2: Energy levels obtained from shell model calculations. The relative strengths of single particle states of ^{209}Pb and ^{209}Bi are normalized to the experimental data of (^{7}Li,^{6}Li) or (^{7}Li,^{6}He) reaction. Each bar represents the strength of a specific configuration and the dashed lines are calculated spectra obtained using the gaussian distribution with the 0.3 MeV FWHM. The overall renomalization is arbitrary. The same colored lines originate from the same single particle state.

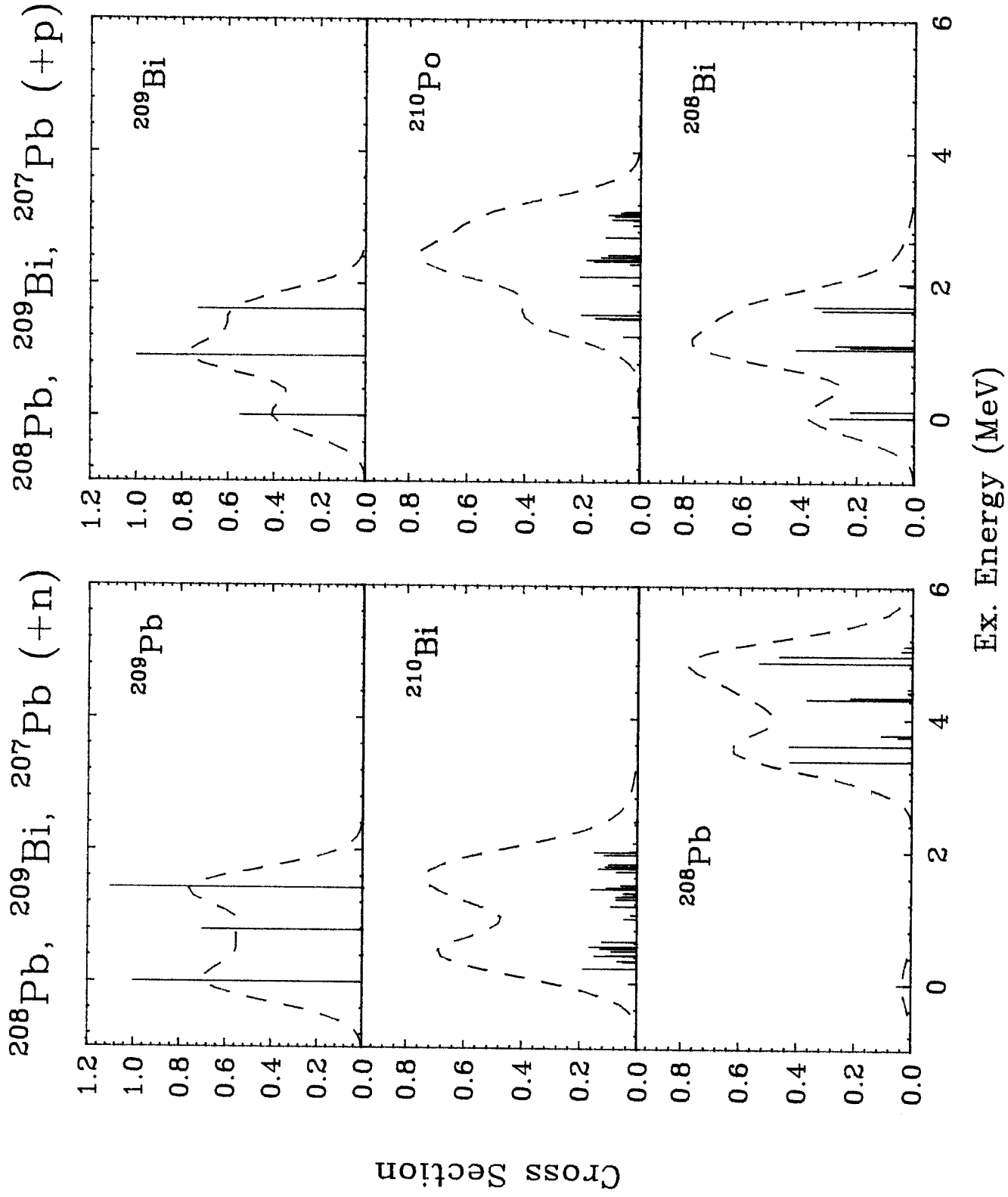
^{208}Pb, ^{209}Bi, ^{207}Pb (+n)
^{209}Pb
^{210}Bi
^{208}Pb
^{208}Pb, ^{209}Bi, ^{207}Pb (+p)
^{209}Bi
^{210}Po
^{208}Bi
Cross Section
Ex. Energy (MeV)

Figure 3.2

Table 3.1: Average excitation energies obtained using shell model calculations for the peaks 1, 2 and 3 of neutron stripping reactions on targets of ^{207}Pb and ^{209}Bi are shown with the experimental data. Each peak is a multiplet between target's state and single particle states where a neutron transferred. The values in parenthesis are the reaction Q – values for the corresponding excitation. Energy levels for the single particle states of the ^{208}Pb$(+n)$ reaction are also given to measure the energy shift from the particle - particle or particle - hole interactions. Experimental errors are about 0.15 MeV.

	Single State	Shell Model Calculations		This Experiment (^7Li, ^6Li)	
Peak #	$^{208}Pb(+n)$ (MeV)	$^{207}Pb(+n)$ (MeV)	$^{209}Bi(+n)$ (MeV)	$^{207}Pb(+n)$ (MeV)	$^{209}Bi(+n)$ (MeV)
1	0. (-3.313) $\nu(g_{9/2})$	3.557 (-3.400) $\nu(p_{1/2})^{-1} \otimes \nu(g_{9/2})$	0.414 (-3.060) $\pi(h_{9/2}) \otimes \nu(g_{9/2})$	3.30 (-3.11)	0.65 (-3.30)
2	0.779 (-4.092) $\nu(i_{11/2})$	4.281 (-4.164) $\nu(p_{1/2})^{-1} \otimes \nu(i_{11/2})$	1.201 (-3.832) $\pi(h_{9/2}) \otimes \nu(i_{11/2})$	4.14 (-4.02)	1.51 (-4.16)
3	1.423 (-4.736) $\nu(j_{15/2})$	4.939 (-4.712) $\nu(p_{1/2})^{-1} \otimes \nu(j_{15/2})$	1.760 (-4.406) $\pi(h_{9/2}) \otimes \nu(j_{15/2})$	4.70 (-4.58)	2.01 (-4.66)

Table 3.2: Average excitation energies obtained using shell model calculations for the peaks 1, 2 and 3 of proton stripping reactions on targets of ^{207}Pb and ^{209}Bi are shown with the experimental data. Each peak is a multiplet between target's state and single particle states where a proton transferred. The values in parenthesis are the reaction Q – values for the corresponding excitation energies. Energy levels for the single particle states of the ^{208}Pb$(+p)$ reaction are also given to measure the energy shift from the particle - particle or particle - hole interactions. Experimental errors are about 0.15 MeV.

	Single State	Shell Model Calculations		This Experiment (^7Li ,^6He)	
Peak	$^{208}Pb(+p)$ (MeV)	$^{207}Pb(+p)$ (MeV)	$^{209}Bi(+p)$ (MeV)	$^{207}Pb(+p)$ (MeV)	$^{209}Bi(+p)$ (MeV)
1	0. (-6.716) $\pi(h_{9/2})$	0.098 (-6.366) $\nu(p_{1/2})^{-1} \otimes \pi(h_{9/2})$	1.479 (-6.270) $\pi(h_{9/2}) \otimes \pi(h_{9/2})$	0.03 (-6.27)	1.39 (-6.38)
2	0.897 (-7.073) $\pi(f_{7/2})$	1.134 (-7.402) $\nu(p_{1/2})^{-1} \otimes \pi(f_{7/2})$	2.354 (-7.324) $\pi(h_{9/2}) \otimes \pi(f_{7/2})$	0.90 (-7.17)	2.12 (-7.11)
3	1.609 (-7.715) $\pi(i_{13/2})$	1.718 (-7.987) $\nu(p_{1/2})^{-1} \otimes \pi(i_{13/2})$	3.002 (-7.980) $\pi(h_{9/2}) \otimes \pi(i_{13/2})$	1.52 (-7.79)	2.73 (-7.72)